Article

Properties of Faint X-ray Activity of XTE J1908+094 in 2019

Debjit Chatterjee [1,2,*], **Arghajit Jana** [3], **Kaushik Chatterjee** [2], **Riya Bhowmick** [2], **Sujoy Kumar Nath** [2], **Sandip K. Chakrabarti** [2], **A. Mangalam** [1] **and Dipak Debnath** [2]

1   Indian Institute of Astrophysics, Koramangala, Bangalore 560034, India; mangalam@iiap.res.in
2   Indian Centre for Space Physics, 43 Chalantika, Garia St. Rd., Kolkata 700084, India;
     mails.kc.physics@gmail.com (K.C.); riyabhowmickmalda@gmail.com (R.B.);
     sujoynath0007@gmail.com (S.K.N.); sandipchakrabarti9@gmail.com (S.K.C.); dipakcsp@gmail.com (D.D.)
3   Physical Research Laboratory, Navrangpura, Ahmedabad 380009, India; argha0004@gmail.com
*   Correspondence: debjit.chatterjee@iiap.res.in

Abstract: We study the properties of the faint X-ray activity of Galactic transient black hole candidate XTE J1908+094 during its 2019 outburst. Here, we report the results of detailed spectral and temporal analysis during this outburst using observations from *Nuclear Spectroscopic Telescope Array (NuSTAR)*. We have not observed any quasi-periodic-oscillations (QPOs) in the power density spectrum (PDS). The spectral study suggests that the source remained in the softer (more precisely, in the soft–intermediate) spectral state during this short period of X-ray activity. We notice a faint but broad Fe Kα emission line at around 6.5 keV. We also estimate the probable mass of the black hole to be $6.5^{+0.5}_{-0.7}\ M_\odot$, with 90% confidence.

Keywords: X-Rays:binaries—stars individual: (XTE J1908+094)—stars:black holes—accretion; accretion disks—shock waves—radiation:dynamics

1. Introduction

Black hole transients (BHTs) are fascinating objects to study. After a long period of quiescence, they show a sudden outburst. The sudden enhancement of viscosity at the piling radius could trigger the outburst [1–3]. The spectral and temporal properties of the source change during the outburst and evolves through the hard state (HS), hard intermediate state (HIMS), soft intermediate state (SIMS), and soft state (SS) [4–6]. Evolution of the state can be seen through hardness intensity diagram (HID) or "q" diagram [7,8] and accretion rate ratio intensity diagram (ARRID; [9,10]). A "failed" outburst is also a commonly known event where the source does not enter the softer spectral states [11–13]. In case of "failed" outbursts, sources do not follow the standard state transition or "q" diagram. The spectral shape varies in different spectral states, mainly due to the relative contribution of the thermal component [14,15] and non-thermal component [16,17].

In Two-Component Advective Flow (TCAF) solution [18,19], the accretion flow consists of two components: high viscous Keplerian flow with high angular momentum and low viscous sub-Keplerian flow with low angular momentum. The sub-Keplerian flow moves towards the black hole almost radially, and it almost stops at the centrifugal barrier and forms an axisymmetric shock [20]. The matter is puffed up beyond the shock and creates a hot electron cloud or Compton corona. This corona is called the CENtrifugal -pressure-supported BOundary Layer (CENBOL). This region intercepts the soft photons coming from the Keplerian disk and emits high-energy photons through inverse-Comptonization. In this way, TCAF can self-consistently explain the accretion dynamics around an accreting black hole. The oscillation of the same shock can explain the observed low-frequency quasi-periodic-oscillations (LFQPOs) [21,22]. The CENBOL is also considered to be the base of jets and outflows [23]. To get an estimation of the physical flow parameters directly from the spectral fit, TCAF model was implemented as an additive table model in XSPEC [24,25]. From spectral fit with the model, we obtain

two accretion rate parameters, namely, the Keplerian disk rate ($\dot{m}_d$) in Eddington rate ($\dot{M}_{Edd}$), the sub-Keplerian halo rate ($\dot{m}_h$) in Eddington rate ($\dot{M}_{Edd}$); two shock or Compton cloud parameters' shock location (X_s) in Schwarzschild radius (r_s), compression ratio (R), which is the ratio between post-shock and pre-shock matter densities ($R = \rho_+/\rho_-$). One can also obtain the best-fitted value of the mass of the black hole (M_{BH} in $M_\odot$) and a normalization parameter from each spectral fit. If the mass of the black hole is well known, it could be kept constant during the spectral fitting.

The Galactic black hole (GBH) candidate XTE J1908+094 was discovered on 21 February 2002 by the Proportional Counter Array (PCA) on-board Rossi X-ray Timing Explorer (*RXTE*) [26]. The source spectrum was fitted with an absorbed power-law with photon index (Γ) of 1.55. The power density spectrum did not show any pulsations and exhibited a flat spectrum between 1 mHz and 0.1 Hz. A broad quasi-periodic-oscillation peak at 1 Hz was observed with a power-law break which continued to 4 Hz. A high-energy cutoff at ∼100 keV was also observed using *BeppoSAX* [27]. The source was suggested to be a black hole (BH) candidate from its spectral and timing properties [26–28]. High inter-stellar absorption (column density, $N_H \sim 2.5 \times 10^{22}$ cm^{-2}) was reported while fitting the spectrum with a multi-color blackbody, a Comptonization and a broad emission line [28]. The dimensionless spin parameter was also measured to be 0.75 from the broadening of Fe Kα line [29].

A radio counterpart was discovered at R.A. = $19^h08^m53.^s07$, DEC. = $+09°23'05''.0$ by *Very Large Array (VLA)* [30] which was also consistent with the Chandra observation [31]. Two possible near-infrared (NIR) counterparts were detected [32,33]—one of them is indicated as an intermediate/late-type (A-K) main-sequence companion, while the other is suggested to be a late-type (later than K) main-sequence secondary star [33]. After two similar outbursts in 2002 and early 2003, XTE J1908+094 went through another outburst on 2013 October 26 [34–38]. The 2013 outburst was well-studied in X-rays by *Swift*, *NuSTAR* [39,40]. Although a relativistic broadening of Fe-Kα line was observed, the spin of the BH could not be constrained due to data quality. A disk reflection contribution was also observed. The source was in the high/soft state during the *NuSTAR* observation. A flare was observed during the studied period. The flare was suggested to be related to the relativistic jet activity. Changes in the corona could be the reason for the flare. Multi-frequency radio and X-ray observation, and radio polarimetry with VLA and AMI-LA during the entire 2013 outburst was done [41]. The source followed the standard hardness-intensity diagram during the outburst. The common behavior of radio jets was also observed, which changes from compact to discrete as the state transits from hard to soft. From the VLBI monitoring of XTE J1908+094, a lateral expansion of resolved, asymmetric jet knots was noticed, which was ejected following the hard- to soft-state transition [42]. The knots are suggested to be the working surface where the ejected materials interacted with the surrounding dense interstellar medium. An external shock formed in this region causes the acceleration of particles, which subsequently diffused outwards over time.

XTE J1908+094 recently showed a "faint" X-ray activity on 2019 April 1 [43]. The source spectrum was fitted with a power-law model with photon index, Γ = 2.3. AMI-LA 15.5 GHz observation on 2019 April 5, detected the radio counterpart of XTE J1908+094 [44]. The obtained spectra on 2019 April 4 from the photon-counting mode of Swift also yield a soft spectrum with high absorption [45]. The source was suggested to be in the soft spectral state while using NICER data on 2019 April 6 and 9 [46].

In this *paper*, we have studied the timing and spectral properties of XTE J1908+094 during its X-ray activity on 2019 April 10 using *NuSTAR* observation of ∼40 ks. The *paper* is organized in the following way. In Section 2, we discuss the observations and the data analysis procedure. In Section 3, we present the temporal and spectral results of our analysis. In Section 4, we carry out the discussion based on our results.

2. Observation and Data Analysis

We processed the *NuSTAR* observation Id 90501317002 (https://heasarc.gsfc.nasa.gov/cgi-bin/W3Browse/w3browse.pl (accessed on 10 April 2019)) using the `nupipeline` command of NuSTAR Data Analysis Software (NuSTARDAS) version 1.8.0 (https://heasarc.gsfc.nasa.gov/docs/nustar/analysis/ (accessed on 10 April 2019)) and with the Calibration database (CALDB) version 1.0.2 (http://heasarc.gsfc.nasa.gov/FTP/caldb/data/nustar/fpm/ (accessed on 10 April 2019)). The spectra and light curves of the source were extracted from the FPMA detectors using a $60''$ circle centered at the position of XTE J1908+094. The background region was selected carefully, since the source could have contamination from the nearby bright source GRS 1915+105. The background was chosen as a $60''$ radius circle as far away from the XTE J1908+094. The background count rate is less than 2% of the source count rate, indicating that the source is still dominant. We also divided the total ~40 ks data in three segments of ~16 ks, ~10 ks, and ~12 ks for detailed study. We used `XSELECT` command `filter time` for this. The spectra and light curves were then generated using `nuproducts`. The spectra were re-binned to have 20 counts/s using `grppha`. The light curves were binned with 100 s time resolution.

For spectral analysis, we used both phenomenological (combined `diskbb`, `powerlaw` models) and physical (TCAF based `fits` file as an additive table model) model in XSPEC version 12.10.1. The hydrogen column density (N_H) was fixed at 2.5×10^{22} cm^{-2} [28]. The multiplicative model, `Tbabs` was used as an absorption table model considering the `vern` scattering cross-sections [47] and `wilm` abundances [48].

3. Results

We studied the 2019 X-ray activity of BHC XTE J1908+094 using *NuSTAR* observation. The source is close to a bright BHC GRS 1915+105. To verify the presence of any contamination due to GRS 1915+105, we studied the source and background count rate variation of XTE J1908+094 (Figure 1). The background count rate was found to be less than 2% of the source count rate. Therefore, we conclude that the X-ray activity of XTE J1908+094 during April 2019 to be "faint" and, yet, the variation observed was inherent rather than due to the nearby sources.
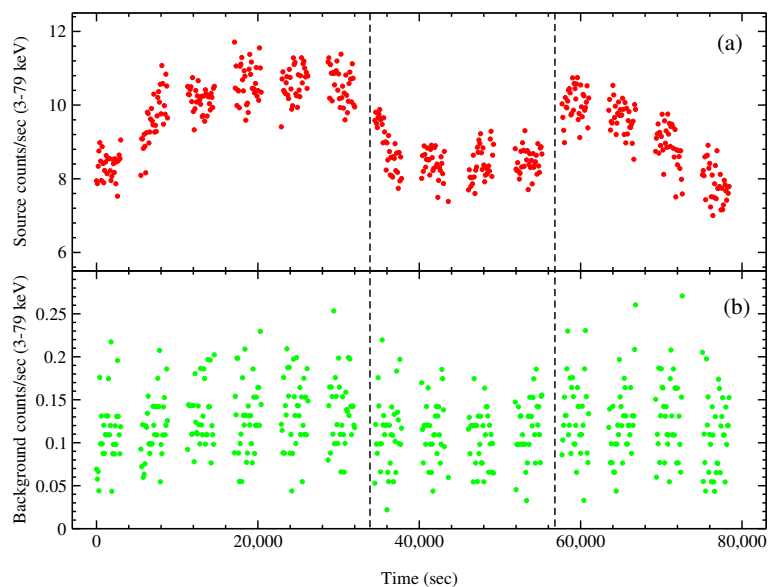

Figure 1. Variation of count rates of XTE J1908+094 from *NuSTAR* observation on 10 April 2019. The upper panel (**a**) shows the count rate for the source and the lower panel (**b**) shows the count rate of the background. The! background count is less than 2% of the source counts.

3.1. Variability Study from the Light Curve

We generated the light curve of 100 s time binning of the total 40 ks data to study the variability (Figure 1a). The light curve shows small variability during this period. We also generated the light curves of 14 individual orbits of 0.01 s time binning. The power density spectra (PDS) do not show any quasi-periodic-oscillations (QPOs). This observation contrasted with the 2002 observations of the object where a broad QPO was observed, and the spectrum was harder [49].

We generated light curves of the entire observation in the energy ranges of 3–10 keV and 10–79 keV. The variation in these light curves, along with the hardness ratio (HR; between 10–79 keV and 3–10 keV), are shown in Figure 2. We noticed that the soft photon (3–10 keV) counts always dominate the hard photon (10–79 keV) counts. Both the soft and hard count rates showed coherent periodic variation during the observation. Thus, the HR always remained at low values (∼0.05 to ∼0.15). The soft and the hard count rates and the value of the HR indicate that the source was in the softer spectral regime during our studied period.
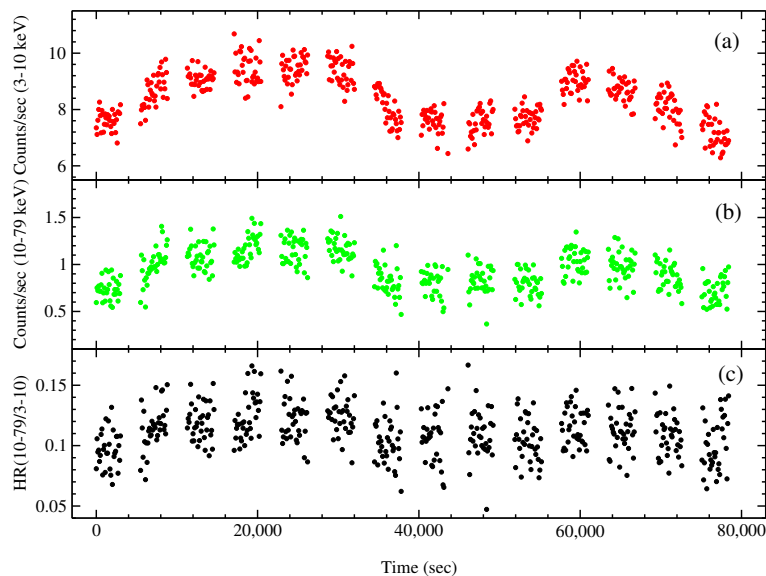

Figure 2. The variation of (**a**) 3–10 keV count rate, (**b**) 10–79 keV count rate, and (**c**) hardness ratio (HR) with time (in sec). The light curves are binned with a time resolution of 100 s.

### 3.2. Accretion Properties from Spectral Analysis

We studied the spectral properties with both phenomenological and physical models separately. We first fitted the spectrum of the full observation (∼40 ks) using combined `diskbb` and `powerlaw` models (Figure 3a). The inner disk temperature (T_{in}) was obtained as 0.779 keV. The high photon index (Γ∼2.085) indicates a softer spectral state. The fitted spectrum retained a χ^2_{red} value of 744/597∼1.246. We noticed a small residual at around 6.5 keV (see Figure 3a). To check the contribution of any Fe-Kα line in the spectrum, we fitted the spectrum with `Tbabs(diskbb+powerlaw+Gaussian)` model (Figure 3b). The inner disk temperature (T_{in}) decreased very little (0.645 keV). The photon index also decreased to (Γ∼2.02). We obtained 6.48 keV as the line energy and ∼1 keV as the line width (σ) from `Gaussian` model. The best fitted spectrum gave a χ^2_{red} value of 549/594∼0.924. The fit improved with the inclusion of the `Gaussian` model for the Fe Kα emission line. We also fitted the spectrum with TCAF `fits` file along with `Gaussian` model (Figure 3c). The disk rate was high ($\dot{m}_d$∼1.699) compared to the halo rate ($\dot{m}_h$∼0.160). The shock location and compression value were obtained as X_s∼49.83 r_s and R∼1.1, respectively. These accretion rates and shock parameters, indicating a softer state, also justify the results obtained from the combined `diskbb+powerlaw+Gaussian` model fitting. The best-fitted spectrum

retained a χ^2_{red} value of 562/592∼0.949. The best-fitted spectra using these three different combinations of models are shown in Figure 3. The spectral parameters are listed in Table 1.
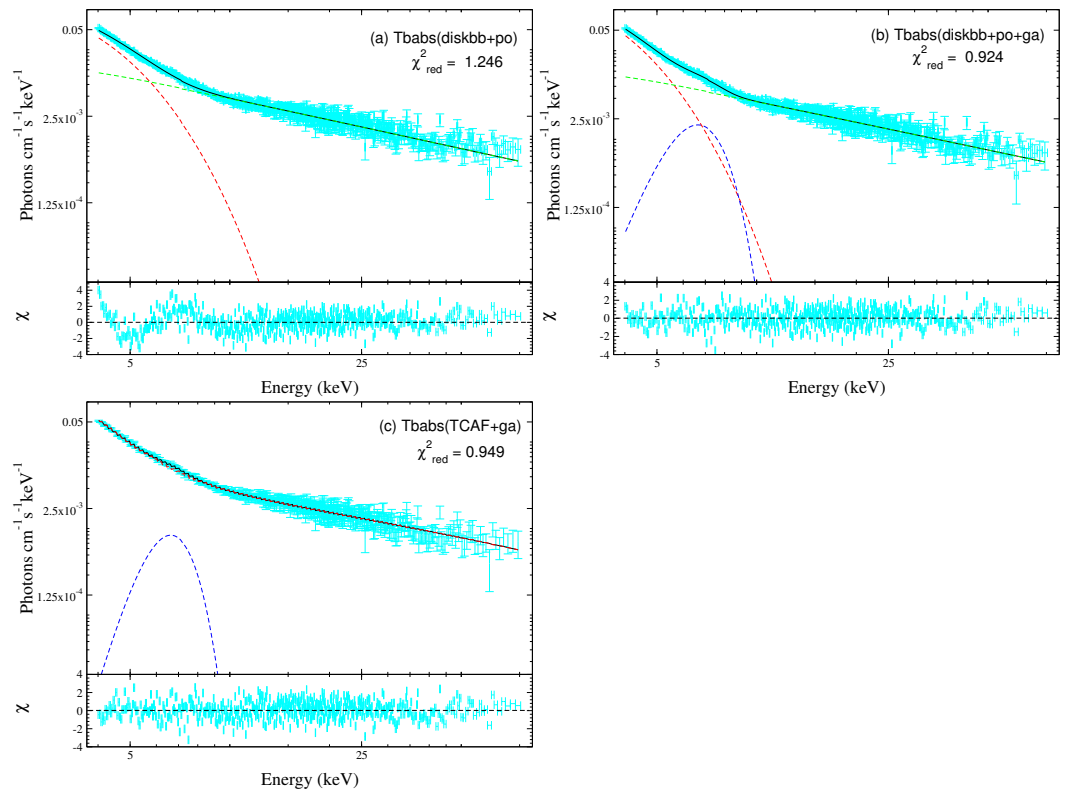
Figure 3. Unfolded spectra using (**a**) `Tbabs(diskbb+powerlaw)`, (**b**) `Tbabs(diskbb+powerlaw+Gaussian)`, and (**c**) `Tbabs(TCAF+Gaussian)` with their ratio. The red, green dashed lines are the `blackbody` and `powerlaw` model components. The solid black line refers to the combined best fitted spectra. The blue dashed lines are the `Gaussian` component.

Since a variation can be easily noticed in the light curve of the full observation (Figure 1a), we divided the light curve into three segments of ∼16 ks, ∼10 ks and ∼12 ks and analyzed for detailed study. We fitted these three spectra using two combinations `Tbabs(diskbb+powerlaw+Gaussian)` and `Tbabs(TCAF+Gaussian)`. The spectral parameters are listed in Table 2. Only TCAF plus Gaussian model fitted spectra are shown in Figure 4.
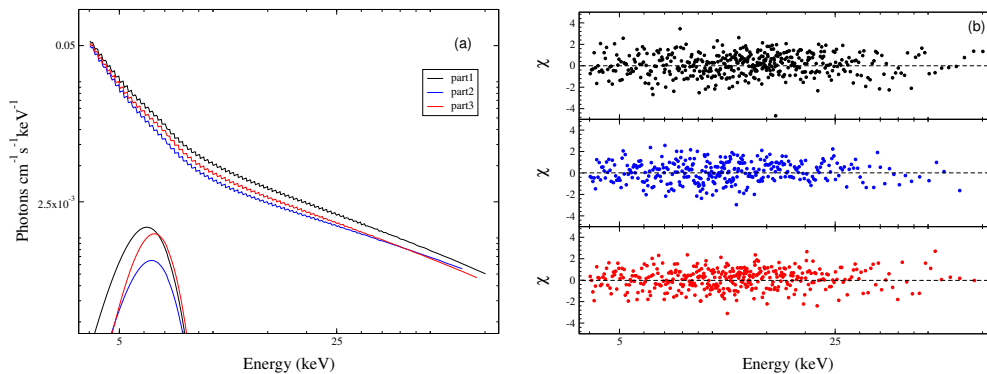
Figure 4. (**a**) **Best-fitted** spectra for the three segments of the *NuSTAR* observation. The right panel (**b**) shows the χ (i.e., (data − model)/error) variations of the three spectra in respective colors.

Table 1. Spectral Analysis Results obtained from *NuSTAR* Observation.

Model1	Diskbb	T_{in} (keV)	$0.779^{+0.013}_{-0.013}$
		norm	153^{+19}_{-16}
	Powerlaw	Γ	$2.085^{+0.028}_{-0.028}$
		norm	$0.057^{+0.004}_{-0.004}$
		χ^2/dof	$744/597 \sim 1.246$
Model2	Diskbb	T_{in} (keV)	$0.645^{+0.019}_{-0.019}$
		norm	493^{+95}_{-72}
	Powerlaw	Γ	$2.023^{+0.028}_{-0.028}$
		norm	$0.047^{+0.003}_{-0.003}$
	Gaussian	E (keV)	$6.483^{+0.152}_{-0.147}$
		σ (keV)	$1.000_{-0.041}$
		norm	$9 \times 10^{-4} \pm 1 \times 10^{-4}$
		χ^2/dof	$549/594 \sim 0.924$
Model3	TCAF	$\dot{m}_d$ ($\dot{M}_{Edd}$)	$1.699^{+0.03}_{-0.04}$
		$\dot{m}_h$ ($\dot{M}_{Edd}$)	$0.160^{+0.03}_{-0.04}$
		X_s (r_s)	49.831^{+9}_{-11}
		R	$1.100^{+0.15}_{-0.16}$
		M_{BH} ($M_{\odot}$)	$6.516^{+0.53}_{-0.76}$
		N_{TCAF}	$312^{+0.08}_{-0.11}$
	Gaussian	E (keV)	$6.521^{+0.183}_{-0.175}$
		σ (keV)	$0.814^{+0.045}_{-0.151}$
		norm	$5 \times 10^{-4} \pm 1 \times 10^{-4}$
		χ^2/dof	$562/592 \sim 0.949$

Table 2. TCAF model fitted spectral parameters for three segments of the *NuSTAR* observation.

	Obs.	**Part1**	**Part2**	**Part3**
	MJD	58,583.471	58,583.709	58,583.975
Diskbb	T_{in} (keV)	$0.652^{+0.033}_{-0.035}$	$0.701^{+0.034}_{-0.032}$	$0.668^{+0.034}_{-0.035}$
	norm	593^{+55}_{-99}	467^{+47}_{-96}	487^{+34}_{-51}
Powerlaw	Γ	$2.084^{+0.043}_{-0.043}$	$1.936^{+0.063}_{-0.063}$	$2.044^{+0.056}_{-0.055}$
	norm	$0.063^{+0.007}_{-0.006}$	$0.032^{+0.005}_{-0.005}$	$0.047^{+0.007}_{-0.006}$
Gaussian	E (keV)	$6.179^{+0.255}_{-0.245}$	$6.768^{+0.311}_{-0.338}$	$6.450^{+0.243}_{-0.227}$
	σ (keV)	$1.000_{-0.088}$	$1.000_{-0.137}$	$1.000_{-0.137}$
	norm	$9 \times 10^{-4} \pm 2 \times 10^{-4}$	$6 \times 10^{-4} \pm 1 \times 10^{-4}$	$9 \times 10^{-4} \pm 2 \times 10^{-4}$
	χ^2/dof	$483/439 \sim 1.100$	$316/332 \sim 0.952$	$352/368 \sim 0.956$
TCAF	$\dot{m}_d$ ($\dot{M}_{Edd}$)	$1.644^{+0.03}_{-0.04}$	$1.572^{+0.03}_{-0.04}$	$1.884^{+0.03}_{-0.04}$
	$\dot{m}_h$ ($\dot{M}_{Edd}$)	$0.137^{+0.03}_{-0.04}$	$0.165^{+0.03}_{-0.04}$	$0.139^{+0.03}_{-0.04}$
	X_s (r_s)	46.117^{+9}_{-11}	50.140^{+9}_{-11}	47.480^{+9}_{-11}
	R	$1.100^{+0.15}_{-0.16}$	$1.101^{+0.15}_{-0.16}$	$1.100^{+0.15}_{-0.16}$
	M_{BH} ($M_{\odot}$)	$6.380^{+0.73}_{-0.66}$	$6.702^{+0.73}_{-0.66}$	$6.721^{+0.53}_{-0.76}$
	N_{TCAF}	$326^{+0.08}_{-0.11}$	$227^{+0.08}_{-0.11}$	$330^{+0.08}_{-0.11}$
Gaussian	E (keV)	$5.959^{+0.297}_{-0.278}$	$6.600^{+0.310}_{-215}$	$6.348^{+0.195}_{-0.201}$
	σ (keV)	$1.000_{-0.145}$	$0.901^{+0.139}_{-0.220}$	$0.900^{+0.099}_{-0.131}$
	norm	$7 \times 10^{-4} \pm 2 \times 10^{-4}$	$3 \times 10^{-4} \pm 3 \times 10^{-5}$	$7 \times 10^{-4} \pm 3 \times 10^{-4}$
	χ^2/dof	$483/437 \sim 1.105$	$321/330 \sim 0.973$	$350/366 \sim 0.956$

3.3. Estimation of Inner Disk Radius and Prediction of Mass

We estimated the mass for XTE J1908-094 from the spectral analysis. From the obtained χ^2_{red} values of model 1 and model 2 in Table 1, we suggested model 2 is the best fitted phenomenological model. We considered the fitted disk-normalization (N_{disk}) to estimate the mass of the BHC XTE J1908+094. We average out the N_{disk} values obtained from fittings of the three segments of the whole observation (Table 2). The inner radius (r_{in}) of the disk and the `diskbb` normalization (N_{disk}) are related, as in

$$N_{disk} = \left(\frac{r_{in}}{D/10 \text{ kpc}}\right)^2 \cos\theta. \tag{1}$$

D is the distance of the system in kpc and r_{in} is in km. θ is the inclination of the disk in degree. This estimated inner radius from the above equation is subjected to some errors (see [50,51]). The corrected inner radius (R_{in} (km)) is,

$$R_{in}(\text{km}) \simeq \kappa^2 \xi r_{in}. \tag{2}$$

κ and ξ are the hardening factor [51] and inner boundary correction factor [50], respectively. Since the inclination angle of the system is not confirmed, we considered three guess values for the inclination as: $\theta \sim 30°$, $50°$, and $80°$. The average value of N_{disk} was 516. We consider the κ and ξ are 1.7 and 0.41, respectively ([50,51]), and assume the distance of the system to be 10 kpc. We obtained the inner radius (R_{in}) for to be 29 km, 34 km, and 65 km, for the inclination angle $30°$, $50°$, and $80°$, respectively. The inner edge of the disk (R_{in}) is considered to be truncated at the inner most stable circular orbit (ISCO). For a Schwarzschild black hole it is $6GM_{BH}/c^2$, where G, M_{BH} and c are the Gravitational constant, mass of the black hole and speed of light at vacuum. We obtained the mass for this black hole from the obtained R_{in} values to be 3.2, 3.7, and 7.2 $M_\odot$, respectively.

In TCAF, the mass of the BH is an important input parameter. If it is not well known from dynamical or other methods, one can obtain the best-fitted value of the M_{BH} from each spectral fit. Here, we obtained the mass of XTE J1908+094 as ~ 6.5 $M_\odot$ from the combined TCAF, and Gaussian model fit when the entire duration of the observation was considered. (Table 1).

4. Conclusions

We studied the spectral and temporal properties of BHC XTE J1908+094 during its renewed X-ray activity using one *NuSTAR* observation in 10 April 2019. The X-ray activity was very faint and mostly dominated by soft photons. No quasi-periodic oscillations (QPOs) were observed in its power density spectra (PDS). The light curves generated in the soft (3–10 keV) and hard (10–79 keV) energy range showed coherent periodic variation. The low value of hardness ratio suggests that the source was in a softer spectral state during the observation.

We analyzed the spectrum using both phenomenological and physical models separately. The high power-law photon index ($\Gamma \sim 2.23$) indicates that the source was either in the soft–intermediate or in soft state. The disk normalization was also relatively high compared to the power-law normalization. Due to the small residual around 6.5 keV, we refitted the spectrum, adding a `Gaussian` for the contribution of Fe Kα line emission. A broad `Gaussian` was obtained with line energy ~ 6.48 keV and line width (σ) ~ 1 keV. The photon index (Γ) decreased to 2.02, suggesting that the source probably was in the soft intermediate state. The presence of a broad width ($\sigma \geq 1$) Gaussian line also signifies the spectral state as soft intermediate. While fitting the three segments of the whole observation divided due to the periodic variability, we noticed that the second segment (see, Table 2) showed a slightly harder spectrum than the other two segments (part1 and part3).

We refitted the spectrum using TCAF plus Gaussian model. We noticed an unusually high disk rate ($\dot{m}_d \sim 1.699$ $\dot{M}_{Edd}$) over the halo rate ($\dot{m}_h \sim 0.160$ $\dot{M}_{Edd}$). This high amount of hard photon contribution is also noticed in the variation in light curves (see, Figure 2).

The obtained shock location ($X_s \sim 49.83 \, r_s$) and compression ratio ($R \sim 1.1$) also refer to soft intermediate spectral state. The spectral parameters obtained from the whole observation's partial fitting also suggest that during the mid-segment, when both soft and hard count decreased, the spectrum became harder but remained in the same spectral state. This faint X-ray activity of XTE J1908+094 in 2019 could be due to the sudden enhancement of viscosity and supply of matter from the pile-up radius. This type of behavior was observed in the case of H1743-322 [2] and GX 339-4 [52]. As the supply of residual matter from the previous outburst (2012–2013) was exhausted, the very short-term X-ray activity was also faded.

We also estimated the possible value of the mass of the black hole (M_{BH}) from the spectral analysis. During our studied period, the spectra are dominated by the soft photons coming from the disk. The inner radius can be constrained in the soft spectral state from the `diskbb` normalization (N_{disk}). Since the other two unknown variables (distance and inclination) are not confirmed for this source, we consider the distance to be 10 kpc and inclination as 30°, 50° and 80°. The corrected inner radius (R_{in}) was obtained as 29 km, 34 km, and 65 km. As the source is found in the soft-intermediate state, the inner radius must be located very close to the ISCO [53]. Considering a Schwarzschild black hole the ISCO is at $\sim \frac{6GM_{BH}}{c^2}$ or 3 r_s. We obtained the black hole mass of 3.2, 3.7 and 7.2 $M_\odot$ for those three R_{in}. This result would only be valid for a Schwarzschild black hole. For a Kerr black hole, the inner radius would be located at less than 3 r_s, affecting the prediction of mass from the disk normalization. We could suggest that the system is located at $\sim$8–10 kpc and is highly inclined (>70°). From the TCAF model fitted spectral fit, we also obtained the mass of the black hole to be $\sim$6.5 $M_\odot$.

5. Summary

We studied the faint outburst of XTE J1908+094 in 2019 using archival *NuSTAR* data. From the timing and spectral study, we conclude that:

(i)   No quasi-periodic oscillation (QPO) was found in the PDS;
(ii)   The source was in SIMS during our studied period;
(iii)   We also estimated the most probable mass of the black hole to be $\sim$6.5 $M_\odot$;

References

1. Chakrabarti, S.K. Grand Unification of Solutions of Accretion and Winds around Black Holes and Neutron Stars. *Astrophys. J.* **1996**, *464*, 664–683. [CrossRef]
2. Chakrabarti, S.K.; Debnath, D.; Nagarkoti, S. Delayed outburst of H 1743-322 in 2003 and relation with its other outbursts. *Adv. Space Res.* **2019**, *63*, 3749–3759. [CrossRef]
3. Mondal, S.; Chakrabarti, S.K.; Nagarkoti, S.; Arévalo, P. Possible Range of Viscosity Parameters to Trigger Black Hole Candidates to Exhibit Different States of Outbursts. *Astrophys. J.* **2017**, *850*, 47–55. [CrossRef]
4. Debnath, D.; Chakrabarti, S.K.; Nandi, A. Evolution of the temporal and the spectral properties in 2010 and 2011 outbursts of H 1743-322. *Adv. Space Res.* **2013**, *52*, 2143–2155. [CrossRef]
5. McClintock, J.E.; Remillard, R.A. *Compact Stellar X-ray Sources*; Cambridge University Press: Cambridge, UK, 2009; pp. 157–214.
6. Remillard, R.A.; McClintock, J.E. X-Ray Properties of Black-Hole Binaries. *Annu. Rev. Astron. Astrophys.* **2006**, *44*, 49–92. [CrossRef]
7. Belloni, T.; Homan, J.; Casella, P.; van der Klis, M.; Nespoli, E.; Lewin, W.H.G.; Miller, J.; Mèndez, M. The evolution of the timing properties of the black-hole transientGX 339-4 during its 2002/2003 outburst. *Astron. Astrophys.* **2005**, *440*, 207–222. [CrossRef]
8. Belloni, T.M. States and Transitions in Black Hole Binaries. In *The Jet Paradigm: From Microquasars to Quasars*; Belloni, T.M., Ed.; Springer: Berlin/Heidelberg, Germany, 2010; Volume 794, pp. 53–84.
9. Jana, A.; Debnath, D.; Chakrabarti, S.K.; Mondal, S.; Molla, A.A. Accretion Flow Dynamics of MAXI J1836-194 During Its 2011 Outburst from TCAF Solution. *Astrophys. J.* **2016**, *819*, 107–117. [CrossRef]
10. Chatterjee, K.; Debnath, D.; Chatterjee, D.; Jana, A.; Chakrabarti, S.K. Inference on accretion flow properties of XTE J1752-223 during its 2009-10 outburst. *Mon. Not. R. Astron. Soc.* **2020**, *493*, 2452–2462. [CrossRef]
11. Chatterjee, D.; Debnath, D.; Jana, A.; Chakrabarti, S.K. Properties of the black hole candidate XTE J1118+480 with the TCAF solution during its jet activity induced 2000 outburst. *Astrophys. Space Sci.* **2019**, *364*, 14. [CrossRef]
12. García, J.A.; Tomsick, J.A.; Sridhar, N.; Grinberg, V.; Connors, R.M.; Wang, J.; Fabian, A. The 2017 Failed Outburst of GX 339-4: Relativistic X-Ray Reflection near the Black Hole Revealed by NuSTAR and Swift Spectroscopy. *Astrophys. J.* **2019**, *885*, 48–59. [CrossRef]
13. Tetarenko, B.E.; Sivakoff, G.R.; Heinke, C.O.; Gladstone, J.C. WATCHDOG: A Comprehensive All-sky Database of Galactic Black Hole X-ray Binaries. *Astrophys. J. Suppl. Ser.* **2016**, *222*, 15–112. [CrossRef]
14. Novikov, I.D.; Thorne, K.S. *Black Holes*; DeWitt, C., DeWitt, B., Eds.; Gordon and Breach: New York, NY, USA, 1973.
15. Shakura, N.I.; Sunyaev, R.A. Black holes in binary systems. Observational appearance. *Astron. Astrophys.* **1973**, *24*, 337–355.
16. Sunyaev, R.A.; Titarchuk, L.G. Comptonization of X-rays in plasma clouds. Typical radiation spectra. *Astron. Astrophys.* **1980**, *86*, 121–138.
17. Sunyaev, R.A.; Titarchuk, L.G. Comptonization of low-frequency radiation in accretion disks Angular distribution and polarization of hard radiation. *Astron. Astrophys.* **1985**, *143*, 374–388. [CrossRef]
18. Chakrabarti, S.K.; Titarchuk, L.G. Spectral Properties of Accretion Disks around Galactic and Extragalactic Black Holes. *Astrophys. J.* **1995**, *455*, 623–639. [CrossRef]
19. Chakrabarti, S.K. Spectral Properties of Accretion Disks around Black Holes. II. Sub-Keplerian Flows with and without Shocks. *Astrophys. J.* **1997**, *484*, 313–322. [CrossRef]
20. Chakrabarti, S.K. *Theory of Transonic Astrophysical Flows*; World Scientific: Singapore, 1990.
21. Molteni, D.; Sponholz, H.; Chakrabarti, S.K. Resonance Oscillation of Radiative Shock Waves in Accretion Disks around Compact Objects. *Astrophys. J.* **1996**, *457*, 805–812. [CrossRef]
22. Nandi, A.; Debnath, D.; Mandal, S.; Chakrabarti, S.K. Accretion flow dynamics during the evolution of timing and spectral properties of GX 339-4 during its 2010-11 outburst. *Astron. Astrophys.* **2012**, *542*, 56–66. [CrossRef]
23. Chakrabarti, S.K. Estimation and effects of the mass outflowfrom shock compressed flow around compact objects. *Astron. Astrophys.* **1999**, *351*, 185–191.
24. Debnath, D.; Mondal, S.; Chakrabarti, S.K. Implementation of two-component advective flow solution in xspec. *Mon. Not. R. Astron. Soc. Lett.* **2014**, *440*, L121–L125. [CrossRef]
25. Debnath, D.; Mondal, S.; Chakrabarti, S.K. Characterization of GX 339-4 outburst of 2010-11: Analysis by XSPEC using two component advective flow model. *Mon. Not. R. Astron. Soc.* **2015**, *447*, 1984–1995. [CrossRef]
26. Woods, P.M.; Kouveliotou, C.; Finger, M.H.; Gogus, E.; Swank, J.; Markwardt, C.; Strohmayer, T. XTE J1908+094. *Int. Astron. Union Circ.* **2002**, *7856*, 1.
27. Feroci, M.; Reboa, L.; BEPPOSAX Team. XTE J1908+094. *Int. Astron. Union Circ.* **2002**, *7861*, 2.
28. Miller, J.M.; Oosterbroek, T.; Parmar, A.N. Broad-band X-ray measurements of the black hole candidateXTE J1908+094. *Astron. Astrophys.* **2002**, *394*, 553–560.
29. Miller, J.M.; Reynolds, C.S.; Fabian, A.C.; Miniutti, G.; Gallo, L.C. Stellar-mass black hole spin constraints from disk reflection and continuum modeling. *Astrophys. J.* **2009**, *697*, 900–912. [CrossRef]
30. Rupen, M.P.; Dhawan, V.; Mioduszewski, A.J. XTE J1908+094. *Int. Astron. Union Circ.* **2002**, *7874*, 1.
31. Jonker, P.G.; Gallo, E.; Dhawan, V.; Rupen, M.; Fender, R.P.; Dubus, G. Radio and X-ray observations during the outburst decay of the black holecandidate XTE J1908+094. *Mon. Not. R. Astron. Soc.* **2004**, *351*, 1359–1364. [CrossRef]

32. Chaty, S.; Mignani, R.P.; Israel, G.L. Discovery of the near-infrared counterpart of the X-ray transient XTE J1908+094. *Mon. Not. R. Astron. Soc.* **2002**, *337*, L23–L26. [CrossRef]

33. Chaty, S.; Mignani, R.P.; Israel, G.L. A closer look at the X-ray transient XTE J1908+094: Identification of two new near-infrared candidate counterparts. *Mon. Not. R. Astron. Soc.* **2006**, *365*, 1387–1391. [CrossRef]

34. Coriat, M.; Tzioumis, T.; Corbel, S.; Fender, R. Optically thin synchrotron emission from XTE J1908+094 observed by the ATCA. *Astron. Telegr.* **2013**, 5575, 1.

35. Krimm, H.A.; Barthelmy, S.D.; Baumgartner, W.; Cummings, J.; Gehrels, N.; Lien, A.Y.; Markwardt, C.B.; Palmer, D.; Sakamoto, T.; Stamatikos, M.; et al. Swift/BAT detects a new outburst from the HXMB/BHC XTE J1908+094. *Astron. Telegr.* **2013**, *5523*, 1.

36. Miller-Jones, J.C.A.; Sivakoff, G.R.; Krimm, H.A. VLA detection of radio emission from the new outburst of XTE J1908+094. *Astron. Telegr.* **2013**, *5530*, 1.

37. Negoro, H.; Suzuki, K.; Ueno, J.S.S.; Tomida, H.; Kimura, M.; Nakahira, S.; Ishikawa, M.; Nakagawa, Y.E.; Mihara, T.; Sugizaki, S.; et al. MAXI/GSC detection of a hard-to-soft state transition of XTE J1908+094. *ATel* **2013**, *5549*, 1.

38. Rushton, A.P.; Fender, R.; Anderson, G.; Staley, T.; Rumsey, C.; Titterington, D. AMI detection of 2 cm radio emission from the XRB BHC J1908+094. *Astron. Telegr.* **2013**, *5532*, 1.

39. Tao L.; Tomsick, J.A.; Walton, D.J.; Fürst, F.; Kennea, J.; Miller, J.M.; Boggs, S.E.; Christensen, F.E.; Craig, W.W.; Gandhi, P.; et al. NuSTAR and Swift Observations of the Black Hole Candidate XTE J1908+094 during its 2013 Outburst. *Astrophys. J.* **2015**, *811*, 51–59. [CrossRef]

40. Zhang, L.; Chen, L.; Qu, J.-L.; Bu, Q.-C.; Zhang, W. The 2013-2014 Outburst of XTE J1908+094 Observed with Swift and NuSTAR: Spectral Evolution and Black Hole Spin Constraint. *Astrophys. J.* **2015**, *813*, 90–102. [CrossRef]

41. Curran, P.A.; Miller-Jones, J.C.; Rushton, A.P.; Pawar, D.D.; Anderson, G.E.; Altamirano, D.; Tudose, V. Radio polarimetry as a probe of unresolved jets: the 2013 outburstof XTE J1908+094. *Mon. Not. R. Astron. Soc.* **2015**, *451*, 3975–3985. [CrossRef]

42. Rushton, A.P.; Miller-Jones, J.C.A.; Curran, P.A.; Sivakoff, G.R.; Rupen, M.P.; Paragi, Z.; Spencer, R.E.; Yang, J.; Altamirano, D.; Belloni, T.; et al. Resolved, expanding jets in the Galactic black hole candidate XTE J1908+094. *Mon. Not. R. Astron. Soc.* **2017**, *468*, 2788–2802. [CrossRef]

43. Rodriguez, J.; Mereminskiy, I.; Grebenev, S.A.; Cangemi, F.; Clavel, M.; Coleiro, A.; Egron, E.; Grinberg, V.; Pottschmidt, K.; Remillard, R.; et al. INTEGRAL detects renewed activity from the microquasar XTE J1908+094. *Astron. Telegr.* **2019**, *12628*, 1.

44. Williams, D.; Motta, S.; Fender, R.; Titterington, D.; Green, D.; Perrott, Y. AMI-LA 15.5 GHz observation of the Black Hole candidate XTE J1908+094. *Astron. Telegr.* **2019**, *12620*, 1.

45. Miller, J.M.; Reynolds, M.; Tetarenko, B.; Ali, S.; Balakrishnan, M.; Chen, J.; Vozza, D. A Neil Gehrels Swift Observatory Snapshot of the Black Hole Candidate XTE J1908+094. *Astron. Telegr.* **2019**, *12632*, 1.

46. Ludlam, R.M.; Remillard, R.; Homan, J.; Strohmayer, T.E.; Gendreau, K.; Arzoumanian, Z. NICER Observations of the new outburst from XTE J1908+094. *Astron. Telegr.* **2019**, *12652*, 1.

47. Verner, D.A.; Ferland, G.J.; Korista, K.T.; Yakovlev, D.G. Atomic Data for Astrophysics. II. New Analytic FITS for Photoionization Cross Sections of Atoms and Ions. *Astrophys. J.* **1996**, *465*, 487–498. [CrossRef]

48. Wilms, J.; Allen, A.; McCray, R. On the Absorption of X-Rays in the Interstellar Medium. *Astrophys. J.* **2000**, *542*, 914–924. [CrossRef]

49. Göğüş, E.; Finger, M.H.; Kouveliotou, C.; Woods, P.M.; Patel, S.K.; Rupen, M.; Van Der Klis, M. Long-term spectral and timing behavior of the black hole candidate XTE J1908+094. *Astrophys. J.* **2004**, *609*, 977–987. [CrossRef]

50. Kubota, A.; Tanaka, Y.; Makishima, K.; Ueda, Y.; Dotani, T.; Inoue, H.; Yamaoka, K. Evidence for a Black Hole in the X-ray Transient GRS 1009-45. *Publ. Astron. Soc. Jpn.* **1998**, *50*, 667–673. [CrossRef]

51. Shimura, T.; Takahara, F. On the Spectral Hardening Factor of the X-Ray Emission from Accretion Disks in Black Hole Candidates. *Astrophys. J.* **1995**, *445*, 780–788. [CrossRef]

52. Bhowmick, R.; Debnath, D.; Chatterjee, K.; Nagarkoti, S.; Chakrabarti, S.K.; Sarkar, R.; Jana, A. Relation Between Quiescence and Outbursting Properties of GX 339-4. *Astrophys. J.* **2021**, *910*, 138. [CrossRef]

53. Done, C.; Gierlinski, M.; Kubota, A. Modelling the behaviour of accretion flows in X-ray binaries: Everything you always wanted to know about accretion but were afraid to ask. *Astron. Astrophys. R* **2007**, *15*, 1–66. [CrossRef]